RSC Advances

PAPER

View Article Online
View Journal | View Issue

Cite this: *RSC Adv.*, 2020, **10**, 16827

Influence of shell thickness on the refractive index sensitivity of localized surface plasmon resonance inflection points in silver-coated gold nanorods†

Kyeong Rim Ryu[a] and Ji Won Ha *[ab]

Silver-coated gold nanorods (Ag@AuNRs) have great potential for biological and chemical sensing, because of their sensitive spectral response to the local environment and unique localized surface plasmon resonance (LSPR) properties. Herein, we investigated the sensitivities of single Ag@AuNRs with different shell thickness with respect to variations in the refractive index (RI) of the surrounding environment. Single Ag@AuNRs with thick shell thickness showed higher RI sensitivity than single Ag@AuNRs with thin shell thickness, which demonstrates the improvement of LSPR sensor due to increase in silver layer thickness. Furthermore, we investigated homogeneous LSPR scattering inflection points (IFs) to better understand the RI sensitivity of single Ag@AuNRs with different Ag shell thickness. The LSPR IFs showed higher RI sensitivity when compared with the frequency shifts of counterpart LSPR peaks observed for single Ag@AuNRs. Finally, single Ag@AuNRs with thick Ag shell demonstrated improved RI sensitivity when compared with single AuNRs with thin Ag shell in the homogeneous LSPR IFs.

Received 23rd March 2020
Accepted 23rd April 2020

DOI: 10.1039/d0ra02691c

rsc.li/rsc-advances

Introduction

Metallic nanoparticles (NPs) show distinct optical properties which are sensitive to their shapes, sizes and refractive index (RI), caused by the localized surface plasmon resonance (LSPR) effect.[1–4] Therefore, in the previous few decades, LSPR in metallic nanoparticles has been widely utilized in applications pertaining to chemical and biological sensors.[5–7] LSPR-based biosensing is based on the sensitivity of the LSPR wavelength to variations in local RI around the nanoparticle surface. The refractive index sensitivity (RIS) aids to measure the displacement in the wavelength shift of the LSPR peak.

Among metallic NPs, gold (Au) and silver (Ag) nanoparticles have demonstrated the most fascinating physical properties with regard to LSPR biosensing.[8,9] AuNPs show good chemical stability and biocompatibility,[10,11] and so they are studied to a large extent in sensing and surface-enhanced Raman scattering (SERS) applications.[12–14] However, for a given shape and size, AgNPs provide better RI sensitivity when compared with AuNPs.[15–17] Nevertheless, AgNPs have been reported to show numerous limitations when utilized for LSPR-based biosensing applications due to their inferior chemical stability and biocompatibility.[18] Recently, many improvements have been achieved with the combination of AgNPs with Au. For instance, mixing Au and Ag to form either alloys or Au–Ag core–shell NPs results in a hybrid LSPR band which can be tailored continuously by controlling the Au–Ag ratio.[6,16]

However, for RI-based LSPR biosensing applications, limited studies have been conducted so far on Au–Ag core–shell NPs by mixing various ratios of Au and Ag. Furthermore, LSPR biosensors are still prone to the occurrence of unsymmetric peak broadening while detecting changes in the local environment at the nanoparticle surface.[19] The unsymmetrical nature of the LSPR peak has the potential to negatively affect sensing efficiency.[20] Recent studies have been conducted to overcome the aforementioned limitation using homogeneous LSPR curvature (or LSPR inflection points, IFs) changes in metallic NPs with respect to local RI changes.[21–23] There have been no studies, however, to elucidate RI sensitivity at LSPR IFs of single Au nanorod (AuNR) coated with versatile Ag shell thickness (Ag@AuNRs).

In this study, a single particle study was presented to reveal the effect of Ag shell thickness on RI sensitivity at LSPR IFs of scattering spectra of single Ag@AuNRs. The RI sensing effect of single Ag@AuNRs embedded in three different surrounding media (air, water, and oil) was studied by dark-field (DF) microscopy and spectroscopy.

Experimental

Characterization of silver-coated gold nanorods

Ag-coated AuNRs with two different shell thickness were purchased from NanoSeedz (Hong Kong, China). Structural

[a]*Advanced Nano-Bio-Imaging and Spectroscopy Laboratory, Department of Chemistry, University of Ulsan, 93 Daehak-ro, Nam-gu, Ulsan 44610, Republic of Korea. E-mail: jwha77@ulsan.ac.kr; Fax: +82 52 712 8002; Tel: +82 52 712 8012*

[b]*Energy Harvest-Storage Research Center (EHSRC), University of Ulsan, 93 Daehak-ro, Nam-gu, Ulsan 44610, Republic of Korea*

† Electronic supplementary information (ESI) available: Supplementary figures and tables. See DOI: 10.1039/d0ra02691c

characterization of Ag@AuNRs with different shell thickness was performed by using transmission emission microscopy (TEM, JEL-2100F, JEOL) to ensure their shapes and sizes. Furthermore, their LSPR absorption spectra in water were measured under a Varian Cary 100 UV-Vis spectroscope (Agilent, USA).

Sample preparation for single particle study

The samples were prepared simply. First, the colloid solution was diluted with pure water to lower the concentration. The diluted solution was sonicated for 10 min at room temperature. Sonicated solution was dropped on the washed slide glass and then covered with 22 mm × 22 mm No. 1.5 cover glass (Corning, NY). To obtain air surrounding medium condition, we dried solution dropped on slide glass after covering with cover glass because solvent of dropped solution is water. In case of oil medium condition after drying solution in the same method of sample preparation with air condition, immersion oil was dropped. In this study, the concentration of Ag@AuNRs deposited on the glass slide was adjusted to be approximately 1 μm^{-2} to minimize inter-particle LSPR coupling and to facilitate measurement of single particle.

Single particle microscopy and spectroscopy

In this study, DF microscopy imaging was used under a Nikon inverted microscope (ECLIPSE Ti-U). In DF mode, the microscope utilized a Nikon Plan Fluor 100× 0.5–1.3 oil iris objective and a Nikon DF condenser. An Andor iXonEM + CCD camera (iXon Ultra 897) was employed to record DF images of Ag@AuNRs. The collected images were analyzed with the Image J software. Furthermore, DF scattering spectra were acquired with an Andor spectrophotometer (SHAMROCK 303i, SR-303I-A) and an Andor CCD camera (Newton DU920P-OE). When recording a spectrum, the scanning stage moved the sample to the desired location was collected by the objective. The scattered light was directed to the entrance of the spectrometer, dispersed by a grating (300 L mm^{-1}) and detected by the Newton CCD camera. The background was measured at a region without nanoparticles. Data analysis on the experimental data was performed by Matlab programs specially designed for this study.

Results and discussion

Transmission electron microscopy (TEM) was used to conduct structural characterizations of Ag@AuNRs in terms of their size and shape. Fig. 1A depicts Ag@AuNRs with two different Ag shell thickness at the same size of AuNR core. Fig. 1B and C show TEM images of Ag@AuNRs with thick shell (thick Ag@AuNRs) and Ag@AuNRs with thin Ag shell (thin Ag@AuNRs), respectively. The difference in the Ag shell thickness between two samples are clearly confirmed in Fig. 1B and C. More TEM images of Ag@AuNRs are provided in Fig. S1.† As shown in Fig. S1,† we noticed that thin Ag@AuNRs had the shapes of cubic and hemisphere at their ends due to heterogeneity issue. But, a majority of thin Ag@AuNRs had the cubic

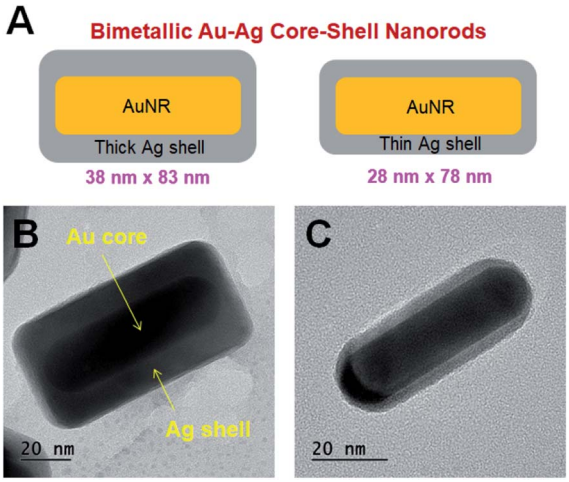

Fig. 1 (A) Schematics to show the size of Au–Ag core–shell nanorods (Ag@AuNRs) with two different shell thickness. (B and C) TEM images of Ag@AuNR with thick Ag shell (B) and Ag@AuNR with thin Ag shell (C).

shape at their ends. As depicted in Fig. 1A, thick Ag@AuNRs were determined to be 83 nm long and 38 nm thick, while thin Ag@AuNRs were 78 nm long and 28 nm thin. In addition, it is notable that, as shown in Fig. S2,† the size of AuNR core (18 nm × 73 nm on average) was same for both of the Ag@AuNR samples. Therefore, we were able to focus on the effect of Ag shell thickness on sensitivity in LSPR-based RI sensing. We then obtained extinction spectra of Ag@AuNRs with two different shell thickness, by using a Varian Cary 300 UV-Vis spectrophotometer (Fig. S3†). The shape-induced distinctive LSPR peaks were observed for Ag@AuNRs dispersed in water. Furthermore, it is notable that the characteristic peaks for Ag are more prominent for Ag@AuNRs with thick shell thickness in the spectral range between 350 nm and 450 nm (Fig. S3A†). However, the ensemble measurements are limited by the lack of homogeneity. Owing to the stated reason, measurement of properties of single particles is necessary to obtain a deeper knowledge of their detailed optical properties.

This study first attempted to elucidate the scattering properties of single Ag@AuNRs under conventional dark-field (DF) microscopy and spectroscopy.[24] The experimental setup for single particle DF microscopy and spectroscopy is shown in Fig. S4.† The sample was obtained by drop casting the Ag@AuNRs in water onto a pre-cleaned glass substrate for DF scattering measurements. Subsequently, the prepared samples were illuminated with a tungsten lamp (white light) focused by an oil-immersion condenser with high numerical aperture (NA) and only the light rays that was scattered from the sample was gathered by the objective lens as depicted in Fig. S5.† The DF scattering image of single Ag@AuNRs with thick shell thickness is presented in Fig. 2A, and the corresponding single particle scattering spectra of four Ag@AuNRs indicated by a green square in (A) are shown in Fig. 2B. As shown in Fig. 2B, the scattering spectra of thick Ag@AuNRs embedded in water showed a broad LSPR peak at about 1.98 eV. Moreover, a scattering image of single Ag@AuNRs with thin shell thickness

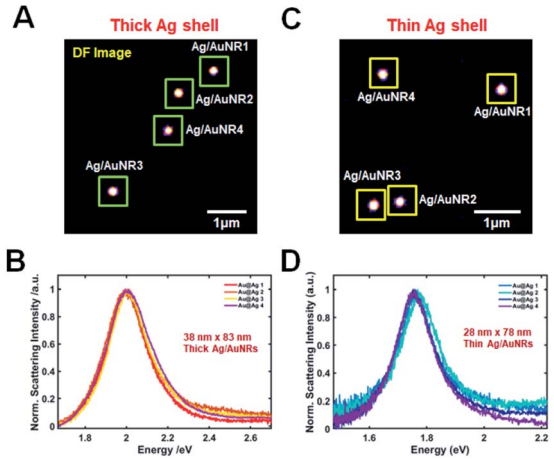

Fig. 2 (A) Dark-field image of single Ag@AuNRs with thick Ag shell. (B) Corresponding scattering spectra of single Ag@AuNRs with thick Ag shell squared with green in (A). (C) Dark-field image of single Ag@AuNRs with thin Ag shell. (D) Corresponding scattering spectra of single Ag@AuNRs with thin Ag shell squared with yellow in (C).

(Fig. 2C) was obtained, and single thin Ag@AuNRs measured in water also exhibited a broad LSPR peak at about 1.77 eV (Fig. 2D).

Subsequently, the influence of changing the RI of the surrounding medium on the LSPR wavelength of Ag@AuNRs having two different shell thickness was investigated. Single particle scattering spectra of Ag@AuNRs were collected in three kinds of RI mediums namely, air, water, and oil. Fig. 3A and B show the scattering spectra of single Ag@AuNRs that have different shell thickness, fixed on a slide and surrounded by air, water, and oil. As seen in Fig. 3A and B, the LSPR wavelengths of a Ag@AuNR increased with increasing the RI from air to oil, which is in good agreement with the earlier studies.[22,25] Fig. 3C presents the comparison of LSPR frequency shifts with respect to the local RI for thick Ag@AuNR (blue-curve) and thin an Ag@AuNR (red-curve). It was confirmed that Ag@AuNR with thick Ag shell showed increased LSPR frequency shift and RI sensitivity than thin Ag@AuNR (Fig. 3C and D). Therefore, the result indicates that single Ag@AuNRs with thick shell thickness yields a higher RI sensitivity in LSPR sensing, which is consistent with the previous results.

It has been reported that in single Au bipyramids with sharp tips the LSPR IFs present superior RI sensitivity when compared with the LSPR wavelength maximum peak.[22] Nevertheless, to the best of our knowledge, there have been no studies to report the RI sensitivity of LSPR curvatures (or IFs) in single Ag@AuNRs with variation in Ag shell thickness. We therefore investigated how the shell thickness affects the RI sensitivity at LSPR IFs while considering the first and second derivatives of homogeneous scattering spectra of Ag@AuNRs.[22] The rows 1–3 in Fig. 4A–C present the scattering spectra of single Ag@AuNR with thick Ag shell and the respective first and second order derivatives. Unlike the rows, the columns are differentiated by three local RI media used, namely, air, water, and oil. The maxima of LSPR scattering peak in the three mentioned RI environments represented by the legend B occurs at 2.17 eV, 2.04 eV, and 1.82 eV for air, water, and oil, respectively. Additionally, the local minima and maxima of the first order derivatives (shown by A and C respectively) occur at 2.09 eV/2.24 eV, 1.98 eV/2.12 eV and 1.75 eV/1.87 eV for the three different RI media, respectively. It is noticed that markers A and C represent

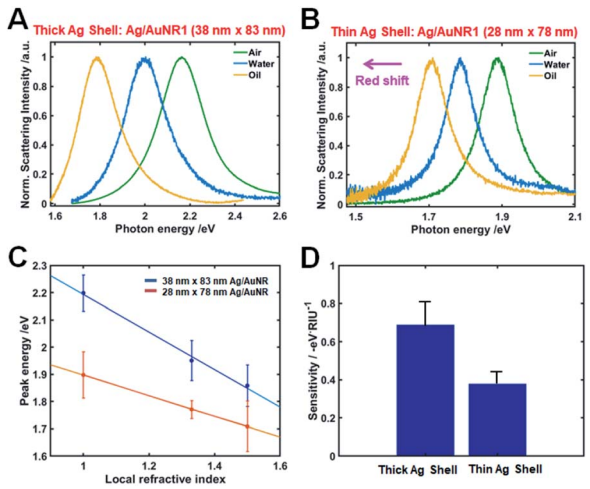

Fig. 3 (A) Change in the LSPR scattering spectra of single Ag@AuNRs with thick Ag shell in the different local RI media, air, water, oil. (B) Change in the LSPR scattering spectra of single Ag@AuNRs with thin Ag shell in the different local RI media, air, water, oil. (C) LSPR wavelength shifts for thick Ag@AuNRs (blue-curve) and thin Ag@AuNRs (red-curve) as a function of the local RI of medium. (D) Comparison of RI sensitivity at the maximum LSPR wavelength for thick Ag@AuNRs (left) and thin Ag@AuNRs (right).

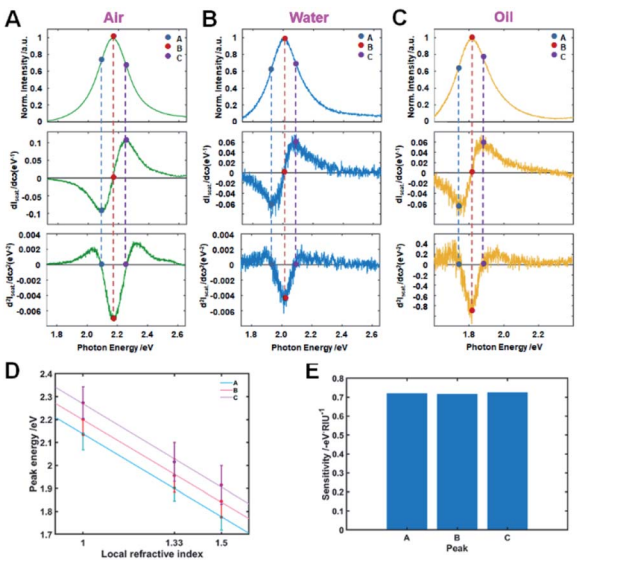

Fig. 4 Inflection point method for single particle LSPR scattering sensing with Ag@AuNRs with thick Ag shell thickness in the three local refractive indexes (air, water, and oil). (A–C) LSPR scattering efficiencies (first row), LSPR scattering efficiencies first order derivatives (second row), and LSPR scattering efficiencies second order derivatives (third row). (D) Peak energy plotted against the three local RI for A, B, and C. (E) Sensitivity of local RI media on peak shifts A, B and C.

the two LSPR IFs which show a value 0 for the second order derivatives of the LSPR scattering spectra (third row). A match between the local minima/maxima of the first order derivatives and the LSPR IFs is observed at the same points of A and C that occur in the photon energy axis for the three RI media considered. Analogous to the first order derivative, the point B appears to be the critical point of LSPR scattering spectra of Ag@AuNR, which represents null value for the first order derivatives spectra.

In our previous report, we presented LSPR IFs collected from extinction spectra of gold nanoparticles recorded at the ensemble level.[16] It is evident from Fig. 4 that the nature of LSPR scattering spectra of single Ag@AuNRs corresponding to the first and second order derivatives collected in this study are in agreement with our previous report. In addition, it is noticed that the first order derivatives records zero perfectly on the point of symmetry for the three local RI media. This point is represented by the legend B which also marks the LSPR peak maxima. An analysis on the curvature confirmed that both the LSPR scattering curves and second order derivatives are even functions that are symmetric about the intensity axis, whereas, the first order derivatives represent odd functions that are symmetrical about the photon energy axis.

In order to confirm the reproducibility and compatibility of the results shown in Fig. 4, we measured and analyzed LSPR scattering spectra of 10 more Ag@AuNRs with thick shell for each local RI environment. The results of these experiments are presented in ESI tables (Tables S1–S3†), which yielded the LSPR peak maxima (B) to be 2.21 (±0.06) eV, 1.96 (±0.06) eV and 1.85 (±0.01) eV for air, water, and oil RI media, respectively. We then determined the values of LSPR IFs to be 2.15 (±0.06) eV (A) and 2.29 (±0.06) eV (C), 1.92 (±0.04) eV (A) and 2.04 (±0.07) eV (C), and 1.78 (±0.05) eV (A) and 1.92 (±0.05) eV (C), respectively. In the regime relevant to sensing properties, we observed that the peak energies show good approximation linear functions of local RI media.[26] We considered A, B, and C peak energies and examined their linearity with respect to local air, water, and oil RI media. Fig. 4D shows plots of energy peaks A, B, and C against local air, water, and oil RI media with corresponding values equal to 1.00, 1.33, and 1.52, respectively. As demonstrated in Fig. 4D, the peak energies at A, B, and C linearized with the local RI media. It should be noted that inflection point C exhibited the highest sensitivity with respect to A and the LSPR peak maxima (B) as shown in Fig. 4E.

To further comprehend the effect of shell thickness on RI sensitivity at the LSPR IFs, Ag@AuNRs with thin shell thickness were measured by scattering-based DF microscopy and spectroscopy. The RI sensitivity of LSPR IFs of thick Ag@AuNRs was then compared with that of thin Ag@AuNRs. Note that both thick Ag@AuNRs and thin Ag@AuNRs have almost same size of AuNR core at the different Ag shell thickness. Therefore, this investigation focuses on influence of the Ag shell thickness of Ag@AuNRs on the RI sensitivity at LSPR IFs at the single particle level.

Similar to the analysis method adopted for thick Ag@AuNRs (Fig. 4), we considered the first and second derivatives of our experimental LSPR scattering spectra of Ag@AuNRs with thin shell. The rows 1–3 shown in Fig. 5A–C present the scattering spectra of single Ag@AuNRs and the respective first and second order derivatives. The maximum peaks of LSPR scattering curve in the three RI environments air, water, and oil are shown by B. It is noticed that they take the values of 1.91 eV, 1.79 eV, and 1.75 eV. The points of local minima and maxima of the first order derivatives flanking the LSPR peak maxima (B) are represented by A/C, situated at values of 1.87 eV/1.94 eV, 1.76 eV/1.83 eV and 1.71 eV/1.78 eV for air, water, and oil mediums. Consequently, A and C show the two LSPR IFs of thin Ag@AuNRs for which the second order derivatives tend to zero.

Same results were recorded when we measured the LSPR (B, maximum) scattering spectra of 10 more Ag@AuNRs for each local RI. The values were calculated to be 1.90 (±0.09) eV, 1.77 (±0.01) eV and 1.74 (±0.04) eV for local air, water, and oil RI, respectively (Tables S4–S6†). Similarly, the LSPR IFs were also computed to be 1.86 (±0.09) eV (A) and 1.94 (±0.09) eV (C), 1.74 (±0.01) eV (A) and 1.81 (±0.02) eV (C), and 1.71 (±0.03) eV (A) and 1.78 (±0.04) eV (C), respectively. We then plotted peak energy A, B, and C as a function of the three selected RI media. As shown in Fig. 5D, the peak energies at A, B, and C revealed a linear behavior with the three selected RI media. Similar to the experimental result of thick Ag@AuNRs in Fig. 4, it is also notable that inflection point C showed the highest sensitivity with respect to the IF A and the LSPR peaks maxima (B) as clearly presented in Fig. 5E. The result is consistent with that of thick Ag@AuNRs in Fig. 4. However, it should be noted that the RI sensitivity at IF C of thick Ag@AuNRs in Fig. 4D was about 2 times higher than that at IF C of thin Ag@AuNRs in Fig. 5E. Therefore, this study found that IF C recorded better RI

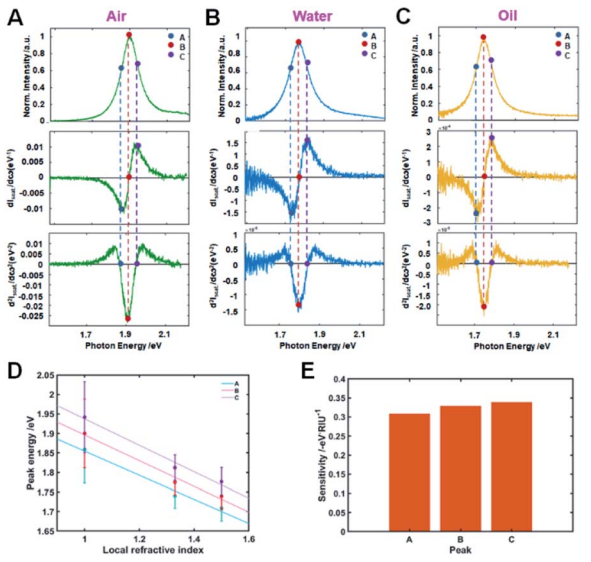

Fig. 5 Inflection point method for single particle LSPR scattering sensing with Ag@AuNRs with thin Ag shell thickness in the three local refractive indexes (air, water, and oil). (A–C) LSPR scattering efficiencies (first row), LSPR scattering efficiencies first order derivatives (second row), and LSPR scattering efficiencies second order derivatives (third row). (D) Peak energy plotted against the three local RI for A, B, and C. (E) Sensitivity of local RI media on peak shifts A, B and C.

sensitivity than the LSPR peak maximum for Ag@AuNRs with two different sizes. Furthermore, thick Ag@AuNRs showed higher RI sensitivity than thin Ag@AuNRs at the locations of LSPR peak maximum (B) and LSPR IFs (A, C) (Fig. 4E and 5E).

Last, we demonstrated the RI sensitivity at the LSPR IFs upon the adsorption of pyridine molecules on thick Ag@AuNRs having higher sensitivity than thin Ag@AuNRs. In this study, we chose pyridine molecules with nitrogen as a target analyte because they are effectively adsorbed on the Ag surface through the nitrogen lone pair (or Ag–nitrogen interaction). After the adsorption of pyridine molecules, the LSPR peak of thick single Ag@AuNR was red-shifted due to the increased local RI around the nanoparticle (Fig. S6A–C†). Furthermore, the IF C showed the highest sensitivity to detect the adsorbate molecules with respect to the IF A and the LSPR peaks maxima (B) as clearly presented in Fig. S6D.† This result is consistent with that of thick Ag@AuNRs in Fig. 4.

Conclusions

In summary, the LSPR sensitivities of single Ag@AuNRs with two different shell thickness towards changes in the three-different surrounding RI media (air, water, oil) were presented. Single Ag@AuNRs with thick shell thickness showed higher RI sensitivity than single Ag@AuNRs with thin shell thickness. Furthermore, higher RI sensitivity was shown at LSPR IF Cs than the variation in the frequency of counterpart LSPR maximum peak for single Au@AuNRs. Therefore, this study provides a deeper insight into the effect of Ag shell thickness on the LSPR RI sensitivity of Ag@AuNRs at LSPR IFs (or curvature). This study further described that homogeneous LSPR IFs in the LSPR scattering spectra of single Ag@AuNRs can be effectively employed for the improvement of sensitivity in LSPR-based RI sensing.

Conflicts of interest

There are no conflicts to declare.

Acknowledgements

This work was supported by a National Research Foundation of Korea (NRF) grant funded by the Korean government (MSIP) (No. 2018R1C1B3001154). This work was also supported by a National Research Foundation of Korea (NRF) grant funded by the Korean government (MSIP) (No. 2019R1A6A1A11053838).

Notes and references

1 C. L. Nehl, H. Liao and J. H. Hafner, *Nano Lett.*, 2006, **6**, 683–688.
2 C. L. Nehl and J. H. Hafner, *J. Mater. Chem.*, 2008, **18**, 2415–2419.
3 I. O. Sosa, C. Noguez and R. G. Barrera, *J. Phys. Chem. B*, 2003, **107**, 6269–6275.
4 M. Hu, J. Chen, Z.-Y. Li, L. Au, G. V. Hartland, X. Li, M. Marquez and Y. Xia, *Chem. Soc. Rev.*, 2006, **35**, 1084–1094.
5 J. N. Anker, W. P. Hall, O. Lyandres, N. C. Shah, J. Zhao and R. P. Van Duyne, *Nat. Mater.*, 2008, **7**, 442–453.
6 A. Loiseau, L. Zhang, D. Hu, M. Salmain, Y. Mazouzi, R. Flack, B. Liedberg and S. Boujday, *ACS Appl. Mater. Interfaces*, 2019, **11**, 46462–46471.
7 A. Loiseau, V. Asila, G. Boitel-Aullen, M. Lam, M. Salmain and S. Boujday, *Biosensors*, 2019, **9**, 78.
8 A. Chen and S. Chatterjee, *Chem. Soc. Rev.*, 2013, **42**, 5425–5438.
9 K. M. Mayer and J. H. Hafner, *Chem. Rev.*, 2011, **111**, 3828–3857.
10 E. Boisselier and D. Astruc, *Chem. Soc. Rev.*, 2009, **38**, 1759–1782.
11 E. C. Dreaden, A. M. Alkilany, X. Huang, C. J. Murphy and M. A. El-Sayed, *Chem. Soc. Rev.*, 2012, **41**, 2740–2779.
12 M. Zhou, M. Li, C. Hou, Z. Li, Y. Wang, K. Xiang and X. Guo, *Chin. Chem. Lett.*, 2018, **29**, 787–790.
13 M. Zhou, M. Lin, L. Chen, Y. Wang, X. Guo, L. Peng, X. Guo and W. Ding, *Chem. Commun.*, 2015, **51**, 5116–5119.
14 M. Zhou, M. Lin, Y. Wang, X. Guo, X. Guo, L. Peng and W. Ding, *Chem. Commun.*, 2015, **51**, 11841–11843.
15 M. Rycenga, C. M. Cobley, J. Zeng, W. Li, C. H. Moran, Q. Zhang, D. Qin and Y. Xia, *Chem. Rev.*, 2011, **111**, 3669–3712.
16 L. Guo, J. A. Jackman, H.-H. Yang, P. Chen, N.-J. Cho and D.-H. Kim, *Nano Today*, 2015, **10**, 213–239.
17 B. Sepúlveda, P. C. Angelomé, L. M. Lechuga and L. M. Liz-Marzán, *Nano Today*, 2009, **4**, 244–251.
18 A. Jakab, C. Rosman, Y. Khalavka, J. Becker, A. Trügler, U. Hohenester and C. Sönnichsen, *ACS Nano*, 2011, **5**, 6880–6885.
19 P. Chen, N. T. Tran, X. Wen, Q. Xiong and B. Liedberg, *ACS Sens.*, 2017, **2**, 235–242.
20 V. Juve, M. F. Cardinal, A. Lombardi, A. Crut, P. Maioli, J. Perez-Juste, L. M. Liz-Marzan, N. Del Fatti and F. Vallee, *Nano Lett.*, 2013, **13**, 2234–2240.
21 P. Chen and B. Liedberg, *Anal. Chem.*, 2014, **86**, 7399–7405.
22 P. V. Tsalu, G. W. Kim, J. W. Hong and J. W. Ha, *Nanoscale*, 2018, **10**, 12554–12563.
23 H. B. Jeon, P. V. Tsalu and J. W. Ha, *Sci. Rep.*, 2019, **9**, 13635.
24 H. B. Jeon and J. W. Ha, *Bull. Korean Chem. Soc.*, 2018, **39**, 1117–1119.
25 W.-S. Chang, J. W. Ha, L. S. Slaughter and S. Link, *Proc. Natl. Acad. Sci. U. S. A.*, 2010, **107**, 2781–2786.
26 A. D. McFarland and R. P. Van Duyne, *Nano Lett.*, 2003, **3**, 1057–1062.